ACS APPLIED MATERIALS & INTERFACES

www.acsami.org Research Article

Dielectric-on-Dielectric Achieved on SiO_2 in Preference to W by Water-free Chemical Vapor Depositions with Aniline Passivation

James Huang, Yunil Cho, Victor Wang, Zichen Zhang, Jing Mu, Ajay Yadav, Keith Wong, Srinivas Nemani, Ellie Yieh, and Kummel Andrew*

Cite This: *ACS Appl. Mater. Interfaces* 2023, 15, 26128−26137 Read Online

ACCESS | Metrics & More | Article Recommendations | Supporting Information

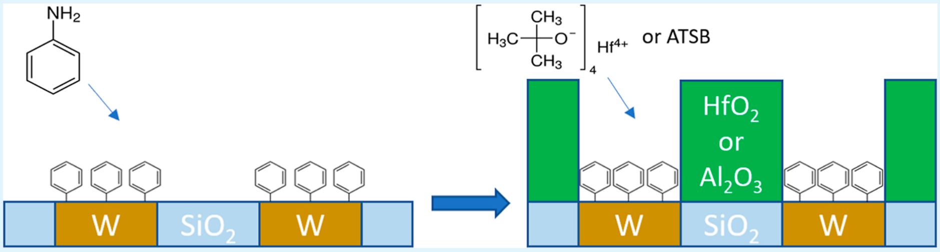

ABSTRACT: Selective and smooth dielectric-on-dielectric was achieved by water-free single-precursor chemical vapor deposition (CVD) processes with the help of aniline passivation. Aniline selective passivation was demonstrated on W surfaces in preference to SiO_2 at 250, 300, and 330 °C. After aniline passivation, selective HfO_2, Al_2O_3, and TiO_2 were deposited only on the HF-cleaned SiO_2 surface by water-free single-precursor CVD using hafnium *tert*-butoxide $Hf(O^tBu)_4$, aluminum-tri-*sec*-butoxide (ATSB), and titanium isopropoxide $Ti(O^iPr)_4$ as the precursor reactants, respectively. $Hf(O^tBu)_4$ and $Ti(O^iPr)_4$ single-precursor CVD was carried out at 300 °C, while the ATSB CVD process was conducted at 330 °C. HfO_2 and Al_2O_3 nanoselectivity tests were performed on W/SiO_2 patterned samples. Transmission electron microscopy images of the W/SiO_2 patterned samples after deposition demonstrated nanoselectivity and low surface roughness of HfO_2 and Al_2O_3 deposition on the SiO_2 regions only.

KEYWORDS: *water-free oxide deposition, area-selective pulsed chemical vapor deposition, hafnium tert-butoxide, aluminum-tri-sec-butoxide, titanium isopropoxide, aniline selective passivation*

1. INTRODUCTION

The current 3-D integrated circuit (IC) requires multilayer circuits bonded together by interconnects. The advantage of 3-D integration comes from the decrease in the interconnect length, which leads to higher performance and lower power consumption.[1−7] Despite the advantages of 3-D IC, it is also facing several challenges such as heat removal, power delivery, and interconnect misalignment.[8,9] This interconnect misalignment is one of the major limitations of IC performance and scaling process due to limited via to metal line distance which leads to shorting or capacitive coupling between the via and the metal.[10]

To solve the interconnect misalignment, Brain et al. first proposed the self-aligned via process to increase the via to metal distance for a 32 nm process.[11] Subsequently, Murdoch et al. and Briggs et al. both described their fully self-aligned via integration processes with metal recess for 5 and 7 nm, respectively.[12,13] Chen et al. proposed the idea of self-aligned via integration using either metal recess etch or dielectric-on-dielectric (DOD) selective deposition.[10] In Chen's paper, metal recess achieved by etch had poor uniformity over the wafer due to an uneven etch rate. DOD selective deposition was the preferred approach which selectively deposits a dielectric buffer layer on top of the existing dielectric to provide the required metal recess.[10] The extra via to metal line distance (x') created by the DOD buffer layer prevented unwanted shorting and capacitive coupling effect and improved the time-dependent dielectric breakdown (shown in Figure 1).

To achieve DOD, area-selective chemical vapor deposition (AS-CVD) or atomic layer deposition (AS-ALD) is required to deposit DOD in preference to metal. AS-CVD can be achieved by three methods: inherent selectivity, selective passivation, and selective activation.[14−16] Inherent selectivity is achieved by the reactivity difference between two substrate surfaces. However, most CVD/ALD processes have deposition on both dielectric and metal surfaces due to their similar surface reactivity. Therefore, self-assembled monolayers (SAMs) or small organic molecule monolayers are typically employed as passivants of the metal surfaces.

Received: February 16, 2023
Accepted: May 5, 2023
Published: May 19, 2023

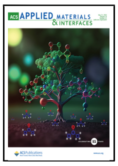

https://doi.org/10.1021/acsami.3c02278
ACS Appl. Mater. Interfaces 2023, 15, 26128−26137

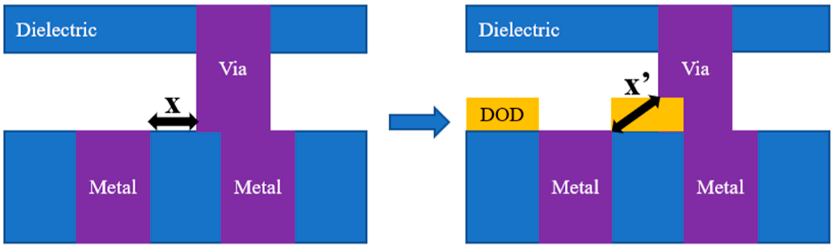

Figure 1. Schematic diagram of DOD increasing the via to line distance by creating metal recess. Interconnect misalignment could be mitigated by employing DOD to achieve a larger via to line distance.

Heshemi et al. and other researchers demonstrated selective passivation on metals and resultant selective DOD deposition by using octadecylphosphonic acid or thiolate as the passivant.[17−19] However, these passivants do not work well with strong oxidizers and are only compatible with low-temperature (<150 °C) ALD, which normally uses water as the co-reactant.[20] This low-temperature water-based ALD might compromise the performance of back-end-of-line (BEOL) circuits by inducing resistor capacitor time delay since a small amount of adsorbed water could lead to a significant increase in the *k* value of low *k* dielectric materials.[21,22]

Another promising metal passivant candidate is aniline. Shearera and Bent showed selective Al_2O_3 deposition on SiO_2 in preference to Cu using nitrogenous aromatic small-molecule inhibitors such as pyrrole, aniline, and pyridine.[23] 3 nm selective Al_2O_3 deposition on SiO_2 was demonstrated using dimethyl aluminum isopropoxide and water at 150 °C. Merkx et al. demonstrated selective TaN ALD on oxide (Al_2O_3/SiO_2) in preference to metal (Ru/Co) with aniline passivation in each ALD cycle. With repetitive aniline passivation and a plasma ALD process, ∼6 nm of selective TaN ALD was achieved on the dielectric at 250 °C. However, selective oxide deposition was not studied in Merkx's paper, and aniline passivation was performed in every cycle of the ALD process. In addition, a plasma process will damage low k dielectrics such as SiCOH.[24,25]

Selective water-free single-precursor HfO_2-pulsed CVD deposition on Si, SiO_2, and SiCOH was previously reported.[26] Selective water-free single-precursor Al_2O_3-pulsed CVD has also been studied by Cho et al. using aluminum-tri-*sec*-butoxide (ATSB) as the precursor.[27] At 300 °C, HfO_2 deposition was achieved by pulsed dosing of the hafnium *tert*-butoxide ($Hf(O^tBu)_4$) precursor. When pulsed gas-phase $Hf(O^tBu)_4$ molecules adsorb onto the substrate surface, it decomposes into HfO/HfOH and $O^tBu/^tBu$ ligands. HfO/HfOH will react with the substrate hydroxyl reactive sites, while remaining ligands will be removed by the nitrogen purge gas. Sequential pulses of $Hf(O^tBu)_4$ induce HfO_2 deposition. At 330 °C, pulsed CVD with ATSB follows the same mechanism and deposits Al_2O_3. The use of multiple short pulses allows time for the precursors to decompose and reaction products to desorb. In the present study, DOD was achieved by the above water-free CVD processes with aniline passivation. Water-free processing is desirable when using low k dielectrics such as SiCOH to ensure that they remain hydrophobic and to avoid oxidation for metal vias and interconnects. Plasma-free processing is also desirable for both conformality and to avoid damage to low-*k* dielectrics.

Even though aniline has been studied as a selective metal passivant in preference to dielectric in several papers, little is known about the water-free plasma-free DOD process and the aniline passivation performance above 250 °C. Therefore, this work seeks to examine the thermal stability of aniline above 250 °C and establish non-destructive BEOL compatible water-free DOD processes.

2. EXPERIMENTAL SECTION

2.1. Reactor. All passivation and CVD processes were carried out in a custom-built vacuum chamber system (see the chamber schematic diagram in Figure S1). It consisted of three major chambers: load-lock chamber (for sample loading and unloading), deposition chamber, and ultra-high vacuum (UHV) chamber. Two or three samples (i.e., W/SiO_2 patterned sample or W, Co, and SiO_2) were simultaneously loaded into the load-lock chamber for a direct selectivity comparison. The deposition chamber has a base pressure of 2×10^{-6} Torr and was used for all the passivation and CVD experiments. This deposition chamber was pumped by a Pfeiffer TPH060 turbo pump with an Edwards RV3 rotary backing pump. Samples were mounted on a copper sample block with a manipulator and a cartridge heater. Samples were heated and located in the center of the deposition chamber during experiments. There was a N_2 purge line, a $Hf(O^tBu)_4$ dosing line, a $Ti(O^iPr)_4$ dosing line, an ATSB dosing line, and an aniline dosing line; all dosing lines were connected to the deposition chamber pointed directly at the sample stage at a distance of 3 in.

2.2. Deposition Process. SiO_2, W, Co, and W/SiO_2 patterned samples were used as the substrate materials. The patterned samples were obtained from Applied Materials (AMAT). For the W/SiO_2 patterned samples, the pitch size was ∼55 nm and the average linewidth was ∼30 nm. TiN was used as a barrier layer between W and SiO_2. All samples were degreased before loading by using acetone, methanol, and HPLC water to rinse for 10 s each. A N_2 air gun was employed after each 10 s rinse to remove the residual solution from the surface. An extra 30 s 0.5% hydrofluoric acid (HF) clean followed by an HPLC water 30 s rinse was performed on SiO_2 only.

Hafnium *tert*-butoxide ($Hf(O^tBu)_4$, 99.99%), ATSB (97%), titanium isopropoxide ($Ti(O^iPr)_4$, 99.99%), and aniline (ACS reagent 99.5%) were purchased from Sigma-Aldrich. For each precursor dosing line, there were at least one pneumatic ALD valve and a shut-off valve except for the $Hf(O^tBu)_4$ dosing line. The $Hf(O^tBu)_4$ dosing line had two pneumatic valves creating a fixed volume in between to achieve a consistent smaller pressure. The N_2 purge line had a leak valve to control the purging pressure. The deposition chamber wall and the dosing lines were heated by heating tapes and kept at 150 °C. No carrier gas was used for any of the precursors.

For HfO_2 and TiO_2 single-precursor CVD processes, experiments were carried out at 300 °C which is the optimized dosing temperature according to previous research.[26,28] For ATSB single-precursor CVD, experiments were conducted at 330 °C for better nucleation and faster growth.[27] Aniline passivation was performed before any CVD processes by trapping the samples inside the deposition chamber (without pumping) for 40 min at 250−350 °C with a constant pressure of 780 mTorr.

For HfO_2 CVD at 300 °C, the $Hf(O^tBu)_4$ precursor bottle was heated to 36 °C. The two pneumatic valves in series were employed to reduce the $Hf(O^tBu)_4$ pulse precursor, and both were set to have an opening time of 500 ms. After the first pneumatic valve opening, $Hf(O^tBu)_4$ gas would flow into the fixed volume tube and be trapped for 10 s. The precursor gas was released by the second pneumatic valve opening with a pressure spike of 0.3 mTorr. Between each fixed volume pulsing, there was a 60 s purge time. A continuous flow of N_2 purge gas was implemented. For Al_2O_3 CVD, the sample stage was heated up to 330 °C. The ATSB precursor bottle was heated to 110 °C. The ATSB dosing line pneumatic valve had an opening time of 200 ms with 10 s purge time between pulses. Each pulse achieved a pressure spike of 0.02 mTorr. During the CVD process, a continuous flow of N_2 purge gas was employed. For TiO_2 CVD, the sample stage was heated to 300 °C. The $Ti(O^iPr)_4$ precursor bottle was kept at room temperature. A pressure spike of 0.1 mTorr was achieved with 200 ms opening time and 5 s purge time between pulses. Continuous N_2 gas was employed.

2.3. Deposition Characterization. Samples were transferred in vacuo to the UHV chamber after deposition. X-ray photoelectron spectroscopy (XPS) was used to perform a compositional study. The XPS system included a monochromatic Al Kα X-ray source (E = 1487 eV) and a hemispherical analyzer (XM 1000 MkII/SPHERA, Omicron Nanotechnology) with a pass energy of 50 eV employed. The XPS anode voltage was set to 10 kV, and the filament emission current was set to 25 mA. All XPS data collected were analyzed by the Casa XPS v2.3 program. Ex situ characterization studies include atomic force microscopy, ellipsometry, transmitted electron microscopy (TEM), and electron energy loss spectroscopy (EELS).

3. RESULTS AND DISCUSSION

3.1. Aniline Passivation at Different Temperatures and on Different Metal Surfaces (W and Co).

The water-free single-precursor HfO_2 CVD was performed on HF-cleaned SiO_2, degreased W, and degreased Co at 300 °C. W and Co are metals known to be easily oxidized and have surface hydroxyl groups. These surface hydroxyl groups will induce the unwanted growth of HfO_2 on these two metals.

Figure 2 shows the growth rate of the water-free single-precursor HfO_2 CVD on unpassivated SiO_2, W, and Co surfaces. After 20 pulses of $Hf(O^tBu)_4$, deposition thicknesses (derived from the equation between the inelastic mean free path and the signal attenuation length of an electron from the substrate) are around 1.4, 1.2, and 0.5 nm on Co, W, and SiO_2, respectively. After a total of 40 pulses, there are 3.3 and 2.2 nm deposition on Co and W, respectively, while only 1.1 nm deposition on SiO_2. Without passivation, HfO_2 deposition growth on Co is around 3 times faster than that on SiO_2. Growth on W is around 2 times faster compared to that on SiO_2. The different growth rates correspond to the oxide bond strength. The cobalt−oxygen bond has the lowest bond energy, while the silicon−oxygen bond possesses the highest bond strength.[29] In sum, precursor molecules more readily chemisorb on the metal surfaces; consequently, SAM or small organic molecules are required to reverse the selectivity.

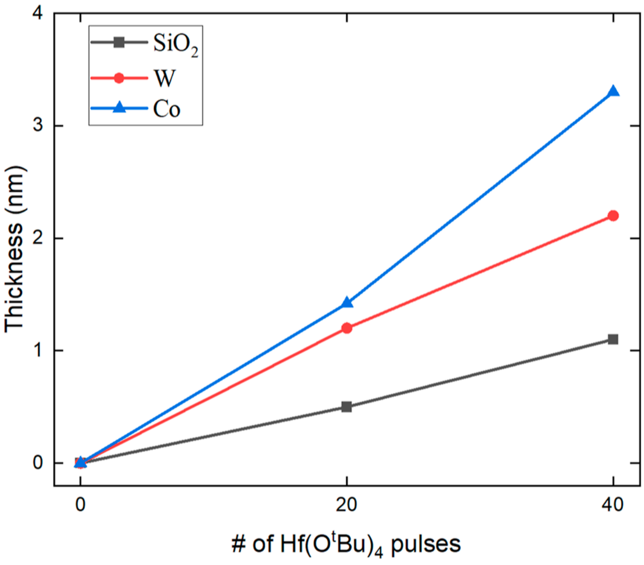

Figure 2. HfO_2 growth curve on SiO_2 vs metals (W and Co). Water-free single-precursor HfO_2 CVD has around 2−3 times faster growth on metals compared to SiO_2.

Merkx et al. performed aniline passivation at the same substrate temperature (250 °C) as their TiN ALD process. Based on Merkx's paper, aniline passivated at 250 °C rendered a satisfactory inhibition of ALD growth on the unwanted area. As a result, aniline passivation at 250 °C was conducted. Samples were trapped in the aniline gas with a pressure of 760 mTorr for 40 min and then followed by $Hf(O^tBu)_4$ dosing at 300 °C.

Selective passivation was achieved on W versus SiO_2 (Figure 3). After the aniline passivation, on the W sample, C_{1s} increased from 0 to 31% and W_{4f} decreased from 48% down to 34%, while no compositional signal change occurred on SiO_2. After aniline passivation, a N_{1s} signal also appeared on W. After 60 pulses of $Hf(O^tBu)_4$, around 3.4 nm was selectively deposited on SiO_2, while 0.1 nm was selectively deposited on W. With an additional 30 pulses of $Hf(O^tBu)_4$, around 7.1 nm (measured by ellipsometry) of HfO_2 was deposited on SiO_2, while only 0.4 nm was deposited on W. Compared to unpassivated W, HfO_2 growth after 60 pulses was inhibited for more than 4.5 nm deposition. Since most of the selective pulsed metal oxide CVD reactions occur at 300 °C, the aniline passivation at 300 °C was also studied.

Figure 4 shows the XPS chemical composition of HF-cleaned SiO_2 and degreased W loaded after a 300 °C rapid UHV annealing, after 40 min 300 °C aniline passivation, and after the pulsed CVD HfO_2 deposition. After aniline passivation, XPS shows that on the W sample, C_{1s} increased from 0 to 26% and W_{4f} decreased from 48% down to 33%, which are similar compared to the 250 °C aniline passivation. This indicated that selective passivation was achieved even at 300 °C. Both aniline passivation at 250 and aniline passivation at 300 °C result in a saturated 0.3 nm carbon monolayer on the W surface. After a total of 100 pulses of $Hf(O^tBu)_4$, similar selectivity was achieved with 7.3 nm HfO_2 deposited on SiO_2, while it was only 0.4 nm on W. This indicated no passivation difference between 250 and 300 °C substrate temperature.

For an effective precursor blocking, both chemical passivation and steric shielding effect need to be considered. For a larger passivant size, steric shielding becomes more prominent.[30] If surface roughness is high, passivant molecules cannot be compactly packed, which leads to a gap between passivant molecules and an early loss in selectivity. The same 300 °C passivation and HfO_2 CVD processes were performed on a rough sputtered W with an RMS roughness of 2.4 nm (W received from AMAT has an RMS roughness of 0.4 nm). Selectivity significantly decreased on the sputtered W due to an increase in RMS roughness (see Supporting Information S4).

The passivation process employed in the above experiments included aniline gas being trapped in the deposition chamber for 40 min at 300 °C. A 60 min trapping time aniline passivation at 300 °C with HfO_2 deposition is shown in Figure S5. Carbon content and selectivity were the same compared to the 40 min passivation. Therefore, 40 min trapping time ensured the saturation of passivation.

40 min 350 °C aniline passivation with HfO_2 CVD at 300 °C was also studied on HF-cleaned SiO_2 and degreased W, as shown in Figure 5. The C_{1s} XPS percentage of the W sample shows a

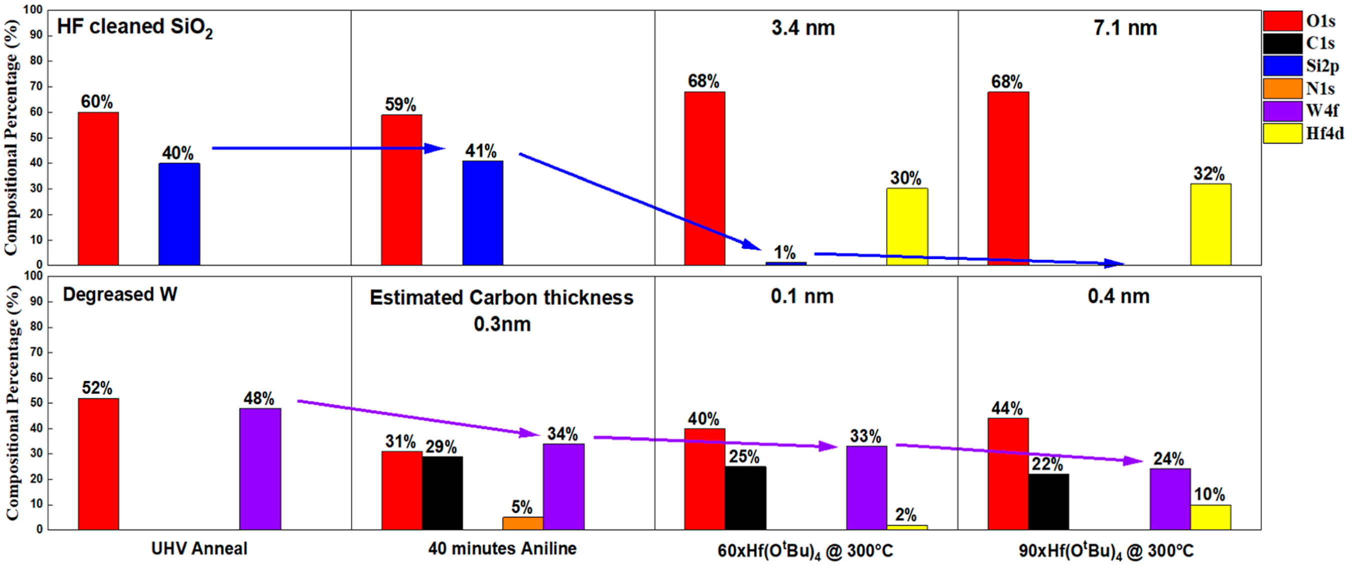

Figure 3. Selective 300 °C HfO_2 CVD on SiO_2 in preference to W with 250 °C aniline passivation. Raw data can be found in Figure S2.

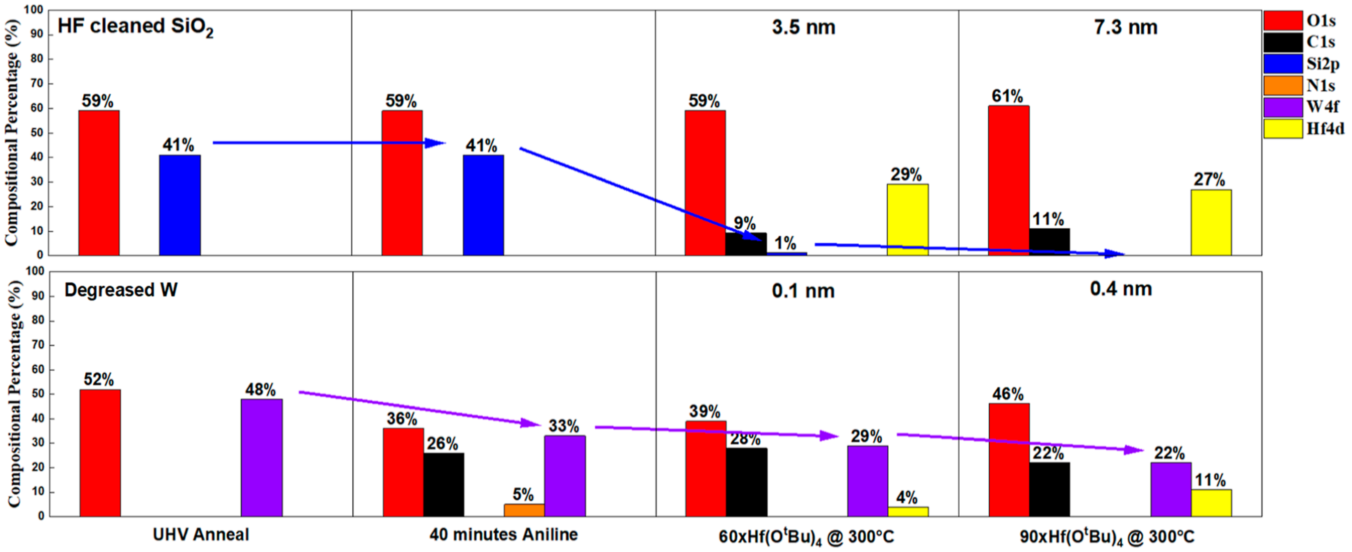

Figure 4. Selective 300 °C HfO_2 CVD on SiO_2 in preference to W with 300 °C aniline passivation. Raw data can be found in Figure S3.

similar percentage increase after aniline dosing compared to the passivation at 250 and 300 °C. Despite the same amount of carbon content initially deposited on the W surface, the C_{1s} percentage decreased noticeably by 9% (28 to 19%) for only a total of 50 $Hf(O^tBu)_4$ pulses. For the 250 and 300 °C aniline passivation, C 1s only went down to 22% after 100/90 $Hf(O^tBu)_4$ pulses. The loss in passivation ability of the 350 °C aniline process could be due to two possible reasons. The diffusion increase resulting from the elevated temperature leads to non-compact aniline monolayer packing, resulting in a less steric shielding effect and lower selectivity. No N_{1s} peak was observed for the W sample after aniline passivation. At 350 °C, aniline might undergo additional decomposition, leading to weak bonding or physisorption between decomposed carbon species and the W surface (without a strong N−metal bond). These weakly bonded carbon species will be easily displaced by the precursor from the pulsed CVD processes. Since aniline has the best passivation performance at 250 and 300 °C, the 300 °C aniline passivation process was employed for additional experiments to maintain the same or similar substrate temperature throughout the experiment.

The optimal passivation and CVD processes were applied on a degreased Co to study the effect of different substrates on the passivation performance.

After aniline passivation, XPS showed a significant increase in the C 1s peak only on Co and not on SiO_2, as shown in Figure 6. C_{1s} of Co increased from 16 to 50%, and Co_{2p} decreased from 34 to 9%. Despite a higher carbon content increase, after a total of 50 pulses of single-precursor $Hf(O^tBu)_4$ CVD, only 2.5 nm was selectively deposited on SiO_2, while 0.3 nm was selectively deposited on Co.

The aniline-passivated W showed a higher selectivity than aniline-passivated Co. This is consistent with the weaker surface oxygen bond (higher surface reactivity) of Co compared to W.[29] According to the DFT calculation from Merkx et al., aniline undergoes two main types of adsorption on metal surfaces.[31] In the first mechanism, aniline absorbs onto metal surfaces through its amine group by forming a N−metal bond. In the second mechanism, aniline bonds to metal surfaces through its phenyl

https://doi.org/10.1021/acsami.3c02278

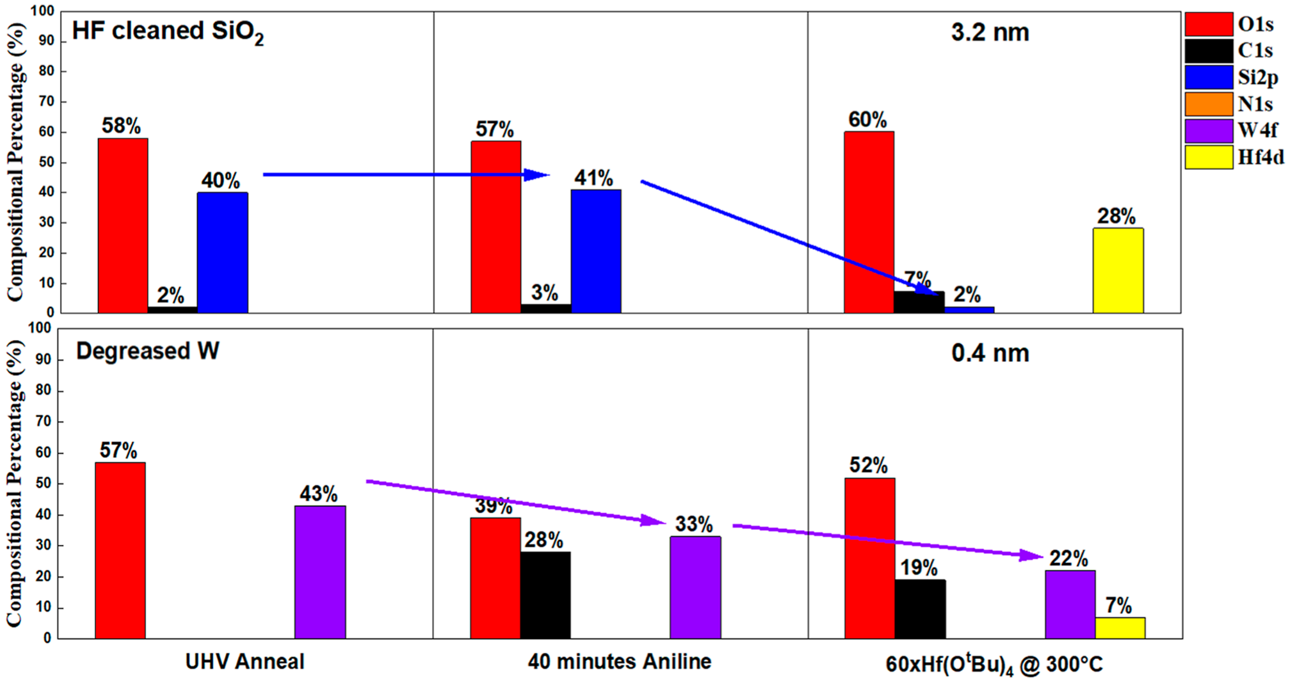

Figure 5. Selective 300 °C HfO_2 CVD on SiO_2 in preference to W with 350 °C aniline passivation. Raw data can be found in Figure S6.

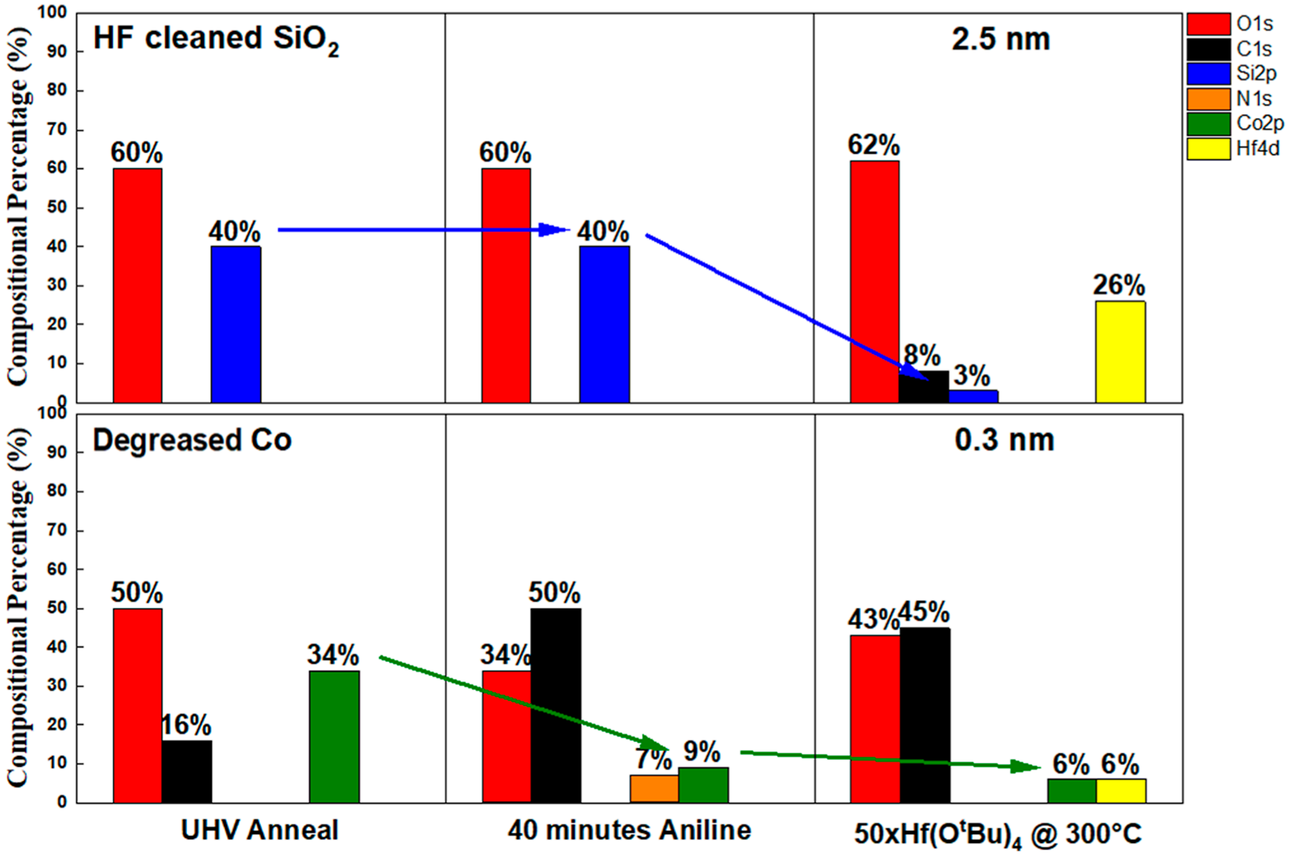

Figure 6. Selective 300 °C HfO_2 CVD on SiO_2 in preference to Co with 300 °C aniline passivation. XPS raw data can be found in Figure S7.

ring with C−metal bonds. Based on the bond dissociation enthalpies, W holds a stronger bond with N and C compared to Co.[32−34] This leads to a stronger passivation on W which corresponds to the higher selectivity observed in the previous studies.

A 330 °C single-precursor Al_2O_3 CVD process using ATSB was also tested with aniline passivation (XPS shown in Figure 7). Due to ATSB's higher decomposition temperature, a substrate temperature of 330 °C was required in the ATSB CVD process to achieve an adequate growth rate. After a total of 400 ATSB

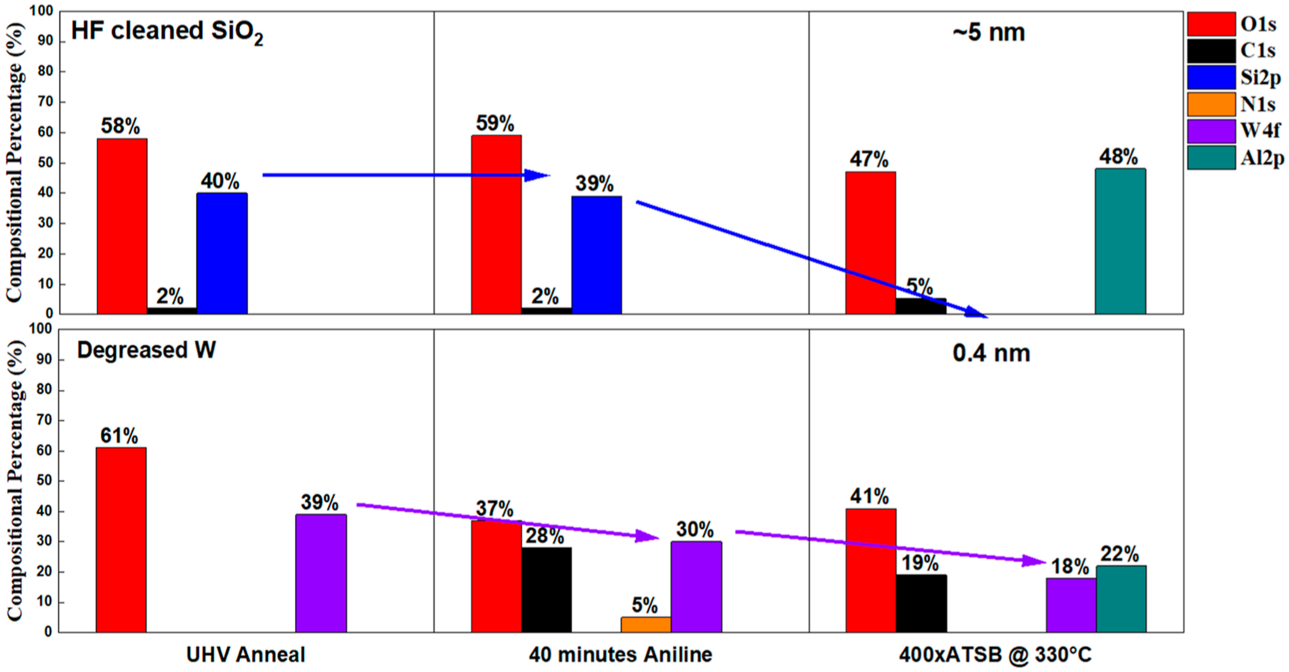

Figure 7. Selective Al_2O_3 330 °C CVD on SiO_2 in preference to W with 300 °C aniline passivation. Raw data can be found in Figure S8.

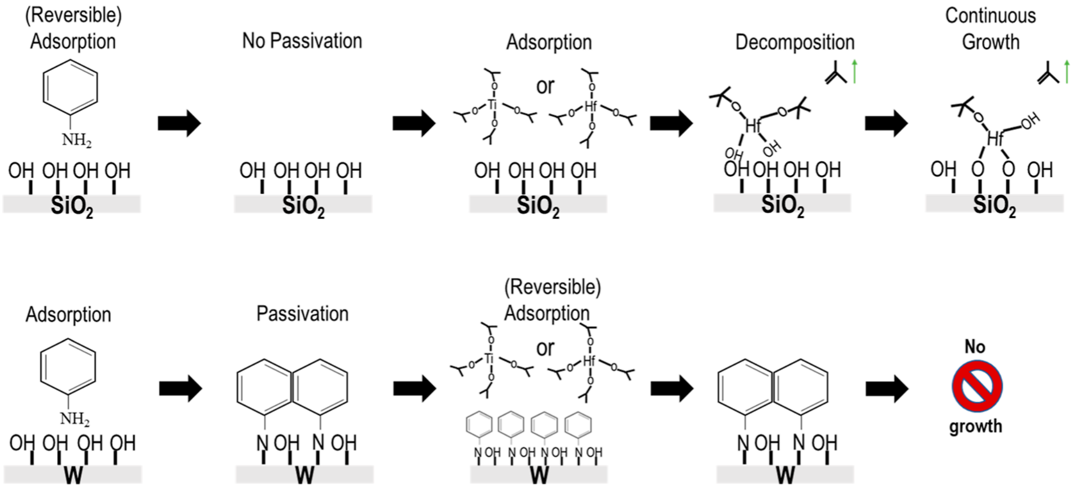

Figure 8. Proposed mechanism of water-free selective single-precursor CVD on SiO_2 in preference to W with 300 °C aniline passivation.

pulses, around 5 nm of Al_2O_3 was selectively deposited on HF SiO_2 in preference to W (0.4 nm). A 300 °C ATSB process after the aniline passivation is shown in Figure S9. Around 3.6 nm of Al_2O_3 was deposited on SiO_2, while 0.4 nm of Al_2O_3 was deposited on W after a total of 640 pulses of ATSB. Based on the XPS data, the lower substrate temperature of the ATSB process resulted in a lower selectivity due to the limited Al_2O_3 growth at 300 °C. A higher number of ATSB pulses was required to deposit the same thickness and resulted in a higher chance of displacing the surface aniline group. The displacement rate depends on the reactivity of the precursor. One typical example is trimethylaluminum (TMA), and TMA is too reactive to be blocked by aniline.[23] By comparing the selectivity result between the 330 and 300 °C ATSB processes, the aniline passivation process is thermally stable at 330 °C and compatible with the 330 °C ATSB CVD process.

In addition, the compatibility test of the 300 °C aniline passivation with the single-precursor TiO_2 CVD process at 300 °C was conducted (as shown in Figure S10). Around 5.1 nm of TiO_2 was grown on HF-cleaned SiO_2, while only 0.3 nm of TiO_2 was deposited on W.

3.2. Mechanism and Nanoselectivity Tests. A proposed mechanism of the water-free single-precursor CVD processes with aniline passivation is shown in Figure 8. Aniline selectively forms a thermodynamically favorable N−metal bond on the W surface. It is hypothesized that with the help of the hydrophobic phenyl ring and its steric shielding, CVD precursors only physisorb on W and desorb at 300 °C. Conversely, CVD precursors chemisorbed onto the SiO_2 surface by reacting with the surface hydroxyl reactive sites. Precursors decompose at 300/330 °C to generate more hydroxyl groups for the sequential pulsing. Thus, continuous CVD growth only occurs on SiO_2, while W remains passivated without deposition.

As shown above, selective pulsed CVD of HfO_2 and Al_2O_3 on blanket SiO_2 in preference to W was documented, but selectivity on the nanoscale can be more challenging since the reaction

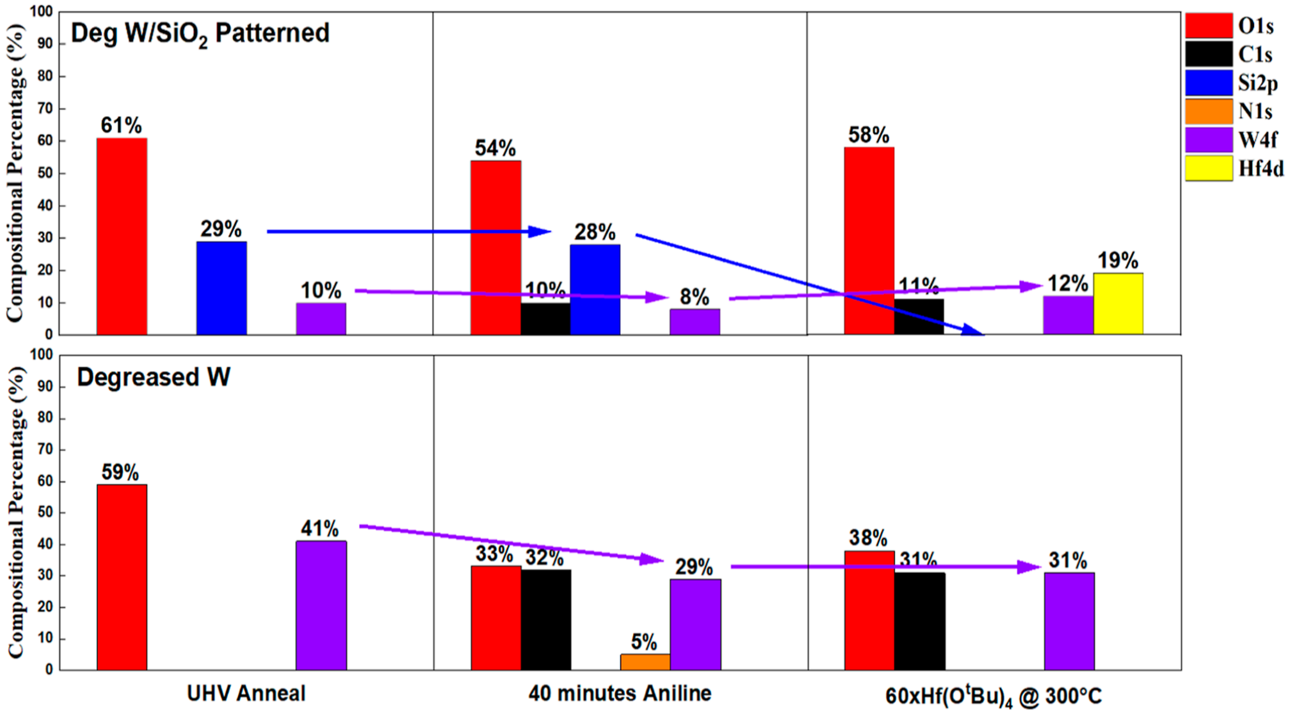

Figure 9. Selective 300 °C HfO_2 CVD on the SiO_2 region of the W/SiO_2 patterned sample with 300 °C aniline passivation. Raw data can be found in Figure S11.

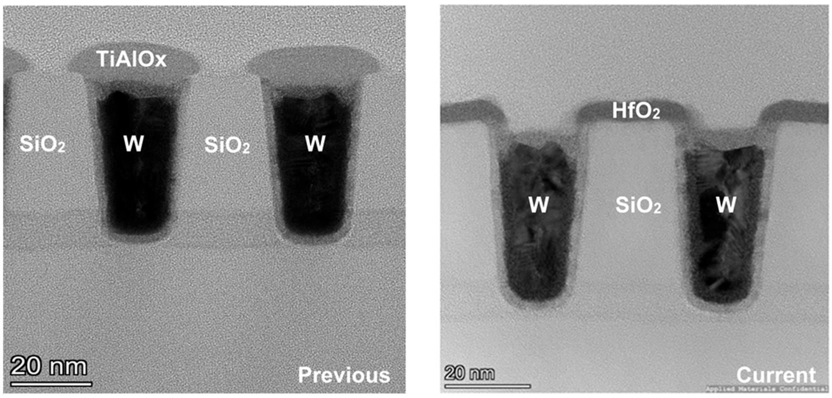

Figure 10. Left: TEM image of a selective 300 °C TiAlO*x* CVD deposition (previously reported) on the W region in preference to SiO_2.[35] Right: selective 300 °C HfO_2 CVD process on the SiO_2 region of the W/SiO_2 patterned sample with the help of 300 °C aniline passivation.

product can diffuse from passivated to unpassivated surfaces. W/SiO_2 patterned samples with a 55 nm pitch size and a linewidth of 30 nm were used to test the nanoselectivity of HfO_2 and Al_2O_3 CVD processes with aniline passivation independently. A W control sample was loaded together with the W/SiO_2 to ensure no HfO_2 deposition on the W region of the patterned sample.

As shown in the XPS in Figure 9, around one monolayer aniline was selectively deposited on the W sample surface after the 40 min aniline passivation. For the patterned sample, the Si_{2p} signal remained unchanged. The C_{1s} peak compositional percentage increased only from 0 to 10%, which is reasonable since the XPS spectra were taken from an array of W and SiO_2 regions. W_{4f} decreased from 10 to 8%, which could be due to the monolayer aniline coverage. No N_{1s} signal was observed from the patterned sample due to the N_{1s} signal being below the XPS detection limit. To prevent overgrowth and secure a clean W region surface, a total of 60 pulses of $Hf(O^tBu)_4$ (less than the number tested on the blanket sample) were employed. The W_{4f} signal increased from 8 to 12%, and this could be due to a different XPS scan region on the patterned sample. Due to micron-size scanning limitation, it became difficult to focus on the exact same W/SiO_2 arrays (nanometer-scale) that have been studied previously. No W signal attenuation was observed on both samples, and no Hf_{4d} signal was detected on the W sample. This indicates a clean and pristine W surface on both the patterned sample and degreased W.

After the HfO_2 CVD deposition with aniline passivation, TEM was performed on the patterned sample. Compared to the previously reported selective TiAlO*x* deposition on W in preference to SiO_2, around 5.5 nm of HfO_2 was selectively deposited on the SiO_2 regions and no deposition was observed on the W regions. As shown in Figure 10, HfO_2 deposition on SiO_2 was uniform and smooth.

As shown in Figure 11, similar XPS results were observed for the ATSB process. Both W/SiO_2 patterned and W samples started with no carbon content on the surface. After the 40 min

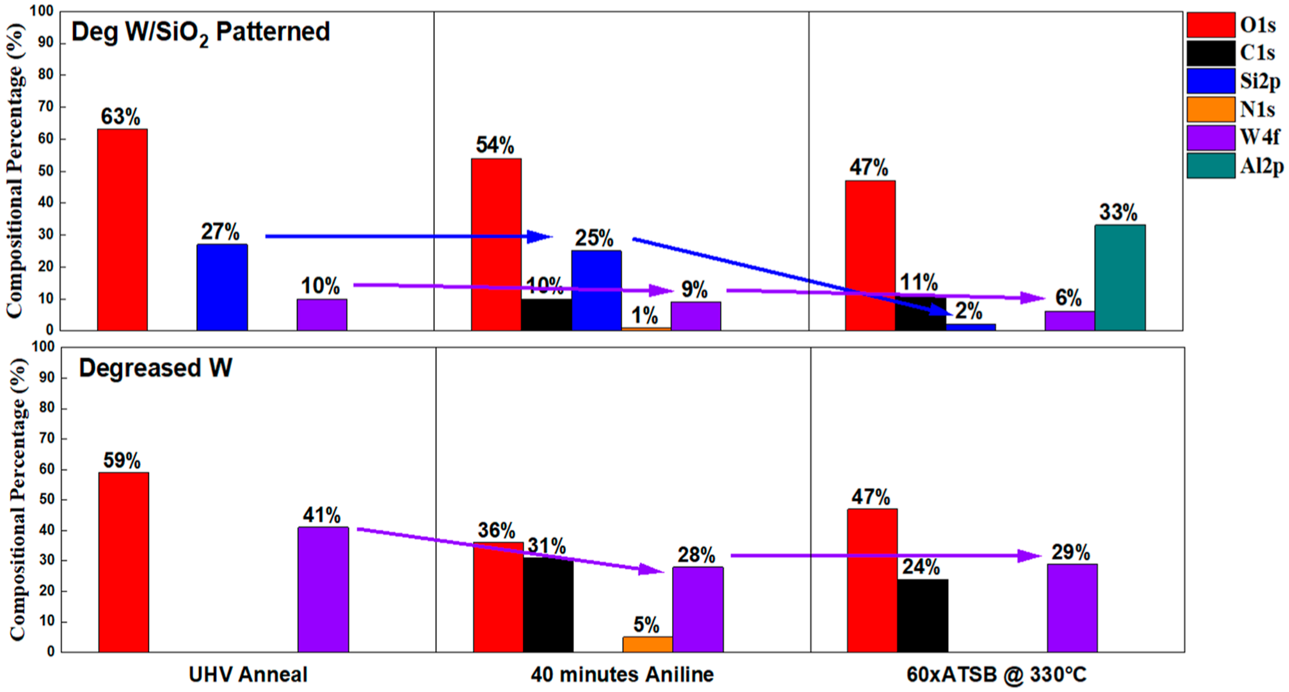

Figure 11. Selective 330 °C Al_2O_3 CVD on the SiO_2 region of the W/SiO_2 patterned sample with 300 °C aniline passivation. Raw data can be found in Figure S12.

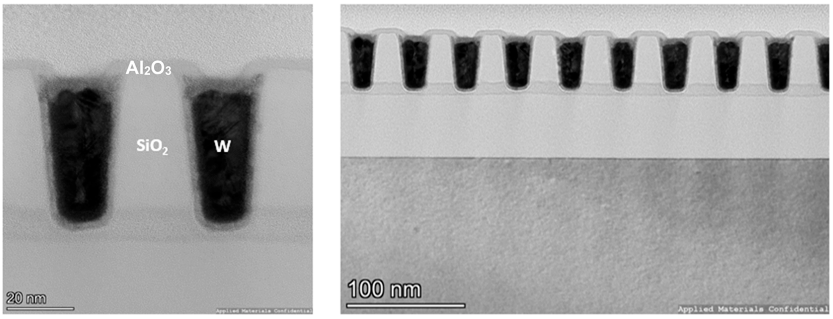

Figure 12. TEM images of the selective 330 °C Al_2O_3 deposition on the SiO_2 region of the W/SiO_2 patterned sample with the help of 300 °C aniline passivation.

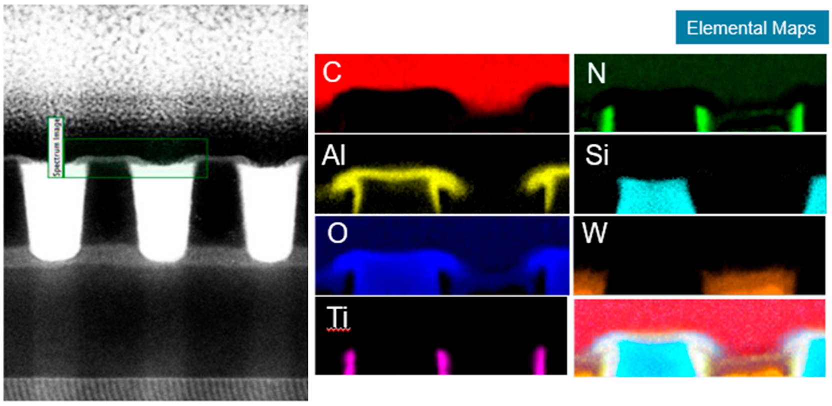

Figure 13. EELS element study proved that Al_2O_3 was selectively deposited on SiO_2.

aniline passivation, around 10% carbon content on the patterned surface was recorded and around 0.3 nm aniline on the blanket W was detected. Only 200 pulses of ATSB were dosed onto the samples to minimize overgrowth on the W region of the patterned sample. After ATSB dosing, the Si_{2p} signal from the patterned sample decreased from 27 to 2%, and the Al_{2p} signal increased from 0 to 33%, while only a 3% decrease was observed for W_{4f}.

As shown in Figure 12, TEM was performed on the W/SiO_2 patterned sample after deposition. Around 4 nm of Al_2O_3 was achieved on the SiO_2 surface, while the W surface remained pristine. A little overgrowth of the Al_2O_3 was observed and covered a portion of the W surface. This overgrowth corresponds to the 3% attenuation in the W_{4f} signal.

EELS was also performed to characterize and identify the surface elements. As shown in Figure 13, the Al signal only appeared on SiO_2 regions, which indicated selective deposition. Al elemental mapping also showed the overgrowth of Al_2O_3. This might be due to the W recess caused by the early CMP process. According to the TEM, around 4 nm of WO*x* was observed on the W surface. This surface WO*x* provides the necessary reactive hydroxyl sites for the CVD processes. The selectivity of the process might increase if this WO*x* layer is removed in situ. As shown in TEM, the Al_2O_3 surface is smooth and uniform throughout the whole sample. Both HfO_2 and Al_2O_3 processes can be used for DOD depending on the preferred *k* value.

4. CONCLUSIONS

Water-free single-precursor CVD tends to grow faster on metal surfaces compared to dielectric surfaces. Aniline can selectively passivate metal surfaces by forming thermodynamically favorable amine metal bonds. The CVD inhibition ability possessed by aniline depends on both chemical passivation and steric shielding effects. Aniline readily passivates W surfaces due to strong bonding and low surface roughness. Aniline passivation can be carried out at 250 or 300 °C but becomes thermally unstable at 350 °C with weaker CVD inhibition ability. With aniline passivation, selective HfO_2, Al_2O_3, and TiO_2 were achieved on HF-cleaned SiO_2 in preference to degreased W by the water-free single-precursor CVD using $Hf(O^tBu)_4$, ATSB, and $Ti(O^iPr)_4$ as the reactants, respectively. Passivation with the ATSB CVD process proved that aniline can be compatible with processes up to 330 °C. HfO_2 and Al_2O_3 nanoselectivity tests were demonstrated on the W/SiO_2 patterned samples. Both processes showed a selective smooth thin film achieved on SiO_2 regions only. With the help of aniline passivation at 300 °C, these water-free single-precursor CVD processes can be the potential solution for BEOL DOD applications.

ASSOCIATED CONTENT

Supporting Information

The Supporting Information is available free of charge at https://pubs.acs.org/doi/10.1021/acsami.3c02278.

> Schematic diagram of the ALD/CVD chamber with the in situ XPS system; raw XPS spectra of Figure 3; raw XPS spectra of Figure 4; selective 300 °C HfO_2 CVD on SiO_2 in preference to sputtered W; selective HfO_2 with 60 min aniline passivation study; raw XPS spectra of Figure 5; raw XPS spectra of Figure 6; raw XPS spectra of Figure 7; selective 300 °C Al_2O_3 CVD with aniline passivation study; selective 300 °C TiO_2 CVD with aniline passivation study; raw XPS spectra of Figure 10; and raw XPS spectra of Figure 11 (PDF)

AUTHOR INFORMATION

Corresponding Author

Kummel Andrew — *Department of Chemistry and Biochemistry, University of California, San Diego, La Jolla, California 92093, United States;* orcid.org/0000-0001-8301-9855; Email: akummel@ucsd.edu

Authors

James Huang — *Materials Science and Engineering, University of California, San Diego, La Jolla, California 92093, United States;* orcid.org/0000-0003-3279-0783

Yunil Cho — *Electrical and Computer Engineering, University of California, San Diego, La Jolla, California 92093, United States;* orcid.org/0000-0002-2680-2015

Victor Wang — *Materials Science and Engineering, University of California, San Diego, La Jolla, California 92093, United States;* orcid.org/0000-0003-1544-2154

Zichen Zhang — *Materials Science and Engineering, University of California, San Diego, La Jolla, California 92093, United States;* orcid.org/0000-0001-8028-3271

Jing Mu — *Materials Science and Engineering, University of California, San Diego, La Jolla, California 92093, United States*

Ajay Yadav — *Applied Materials, Inc., Santa Clara, California 95054, United States*

Keith Wong — *Applied Materials, Inc., Santa Clara, California 95054, United States*

Srinivas Nemani — *Applied Materials, Inc., Santa Clara, California 95054, United States*

Ellie Yieh — *Applied Materials, Inc., Santa Clara, California 95054, United States*

Complete contact information is available at: https://pubs.acs.org/10.1021/acsami.3c02278

Notes

The authors declare no competing financial interest.

ACKNOWLEDGMENTS

Funding support from Applied Materials is gratefully acknowledged. The ellipsometry measurements were facilitated by the San Diego Nanotechnology Infrastructure (SDNI) which is supported by the National Science Foundation (NSF) to Nano3 (grant ECCS-1542148).

REFERENCES

(1) Joyner, J.; Venkatesan, R.; Zarkesh-Ha, P.; Davis, J.; Meindl, J. Impact of Three-Dimensional Architectures on Interconnects in Gigascale Integration. *IEEE Trans. Very Large Scale Integr. (VLSI) Syst.* **2001**, *9*, 922−928.

(2) Joyner, J. W.; Zarkesh-Ha, P.; Meindl, J. A Stochastic Global Net-Length Distribution for A Three-Dimensional System-On-A-Chip (3D-SoC). *14th Annual IEEE International ASIC/SOC Conference*; IEEE Cat. no. 01TH8558, 2001; pp 147−151.

(3) Nahman, A.; Fan, A.; Chung, J.; Reif, R. Wire-Length Distribution of Three-Dimensional Integrated Circuits. *1999 IEEE International Interconnect Technology Conference (Cat. No. 99EX247)*, 1999; pp 233−235.

(4) Rahman, A.; Reif, R. System-Level Performance Evaluation of Three-Dimensional Integrated Circuits. *IEEE Trans. Very Large Scale Integr. (VLSI) Syst.* **2000**, *8*, 671−678.

(5) Pavlidis, V.; Friedman, E. Interconnect-Based Design Methodologies for Three-Dimensional Integrated Circuits. *IEEE* **2009**, *97*, 123−140.

(6) Joyner, J.; Meindl, J. Opportunities for Reduced Power Dissipation Using Three-Dimensional Integration. *IEEE 2002 International Interconnect Technology Conference* (Cat no. 02EX519), 2002, pp 148−150.

(7) Zhang, R.; Roy, K.; Koh, C.; Janes, D. Stochastic Interconnect Modeling, Power Trends, and Performance Characterization of 3-D Circuits. *IEEE Trans. Electron Devices* **2001**, *48*, 638−652.

(8) Kumar, V.; Naeemi, A. An Overview of 3D Integrated Circuits, *2017 IEEE MTT-S International Conference on Numerical Electro-*

magnetic and Multiphysics Modeling and Optimization for RF, Microwave, and Terahertz Applications (NEMO), 2017; pp 311−313.

(9) Jani, I.; Lattard, D.; Vivet, P.; Arnaud, L.; Beigné, E. Misalignment Analysis and Electrical Performance of High Density 3D-IC Interconnects. *2019 International 3D Systems Integration Conference (3DIC)*, 2019; pp 1−4.

(10) Chen, H.; Wu, Y.; Huang, H.; Tsai, C.; Lee, S.; Lee, C.; Wei, T.; Yao, H.; Wang, Y.; Liao, C.; Chang, H.; Lu, C.; Shue, W.; Cao, M. Fully Self-Aligned via Integration for Interconnect Scaling beyond 3 nm Node. *2021 IEEE International Electron Devices Meeting (IEDM)*, 2021; pp 22.1.1−22.1.4.

(11) Brain, R.; Agrawal, S.; Becher, D.; Bigwood, R.; Buehler, M.; Chikarmane, V.; Childs, M.; Choi, J.; Daviess, S.; Ganpule, C.; He, J.; Hentges, P.; Jin, I.; Klopcic, S.; Malyavantham, G.; McFadden, B.; Neulinger, J.; Neirynck, J.; Neirynck, Y.; Pelto, C.; Plekhanov, P.; Shusterman, Y.; Van, T.; Weiss, M.; Williams, S.; Xia, F.; Yashar, P.; Yeoh, A. Low-K Interconnect Stack with A Novel Self-Aligned via Patterning Process for 32nm High Volume Manufacturing. *2009 IEEE International Interconnect Technology Conference*, 2009; pp 249−251.

(12) Murdoch, G.; Bommels, J.; Wilson, C.; Gavan, K.; Le, Q.; Tokei, Z.; Clark, W. Feasibility Study of Fully Self Aligned Vias for 5nm Node BEOL. *2017 IEEE International Interconnect Technology Conference (IITC)*, 2017; pp 1−4.

(13) Briggs, B.; Peethala, C.; Rath, D.; Lee, J.; Nguyen, S.; LiCausi, N.; McLaughlin, P.; You, H.; Sil, D.; Lanzillo, N.; Huang, H.; Patlolla, R.; Haigh, T.; Xu, Y.; Park, C.; Kerber, P.; Shobha, H.; Kim, Y.; Demarest, J.; Li, J.; Lian, G.; Ali, M.; Le, C.; Ryan, E.; Clevenger, L.; Canaperi, D.; Standaert, T.; Bonilla, G.; Huang, E. Fully Aligned via Integration for Extendibility of Interconnects to beyond the 7 nm Node. *2017 IEEE International Electron Devices Meeting (IEDM)*, 2017; pp 14.2.1−14.2.4.

(14) Yang, M.; Aarnink, A.; Schmitz, J.; Kovalgin, A. Y. Inherently Area-Selective Hot-Wire Assisted Atomic Layer Deposition of Tungsten Films. *Thin Solid Films* **2018**, *649*, 17−23.

(15) Choi, J. Y.; Ahles, C. F.; Wong, K. T.; Nemani, S.; Yieh, E.; Kummel, A. C. Highly Selective Atomic Layer Deposition of MoSiOx Using Inherently Substrate-Dependent Processes. *Appl. Surf. Sci.* **2020**, *512*, 144307.

(16) Lemaire, P. C.; King, M.; Parsons, G. N. Understanding Inherent Substrate Selectivity During Atomic Layer Deposition: Effect of Surface Preparation, Hydroxyl Density, and Metal Oxide Composition on Nucleation Mechanisms During Tungsten ALD. *J. Chem. Phys.* **2017**, *146*, 052811.

(17) Hashemi, S. M.; Prasittichai, C.; Bent, S. A New Resist for Area Selective Atomic and Molecular Layer Deposition on Metal−Dielectric Patterns. *J. Phys. Chem. C* **2014**, *118*, 10957−10962.

(18) Pasquali, M.; De Gendt, S.; Armini, S. Area-Selective Deposition by A Combination of Organic Film Passivation and Atomic Layer Deposition. *ECS Trans.* **2019**, *92*, 25−32.

(19) Liu, T. L.; Nardi, K. L.; Draeger, N.; Hausmann, D. M.; Bent, S. Effect of Multilayer Versus Monolayer Dodecanethiol on Selectivity and Pattern Integrity in Area-Selective Atomic Layer Deposition. *ACS Appl. Mater. Interfaces* **2020**, *12*, 42226−42235.

(20) Liu, G.; Kanjolia, R.; Potyen, M.; Woodruff, J.; Zope, B.; Chandra, H.; Lei, X. Selective Deposition of Dielectric on Dielectric Using Low Temperature ALD SiO2 from A Halogen-Free Precursor. *ASD2022*, 2022; p 11.

(21) Shamiryan, D.; Abell, T.; Iacopi, F.; Maex, K. Low-K Dielectric Materials. *Mater. Today* **2004**, *7*, 34.

(22) Lee, W.; Fukazawa, A.; Choa, Y. H. Gap-Fill Characteristics and Film Properties of DMDMOS Fabricated by An F-CVD System. *Korean J. Mater. Res.* **2016**, *26*, 455−459.

(23) Shearera, A.; Bent, S. Area-Selective Atomic Layer Deposition Using Nitrogenous Aromatic Small Molecule Inhibitors. *ASD2022*, 2022.

(24) Merkx, M. J. M.; Vlaanderen, S.; Faraz, T.; Verheijen, M. A.; Kessels, W. M. M.; MacKus, A. J. M. Area-Selective Atomic Layer Deposition of TiN Using Aromatic Inhibitor Molecules for Metal/Dielectric Selectivity. *Chem. Mater.* **2020**, *32*, 7788−7795.

(25) Oszinda, T.; Schaller, M.; Schulz, S. E. Chemical Repair of Plasma Damaged Porous Ultra Low-K SiOCH Film Using A Vapor Phase Process. *J. Electrochem. Soc.* **2010**, *157*, H1140.

(26) Choi, J. Y.; Ahles, C. F.; Cho, Y.; Anurag, A.; Wong, K. T.; Nemani, S. D.; Yieh, E.; Kummel, A. Selective Pulsed Chemical Vapor Deposition of Water-Free HfOx on Si in Preference to SiCOH and Passivated SiO2. *Appl. Surf. Sci.* **2020**, *512*, 145733.

(27) Cho, Y.; Huang, J.; Zhang, Z.; Wang, K.; Lee, P.; Kim, C.; Wong, K.; Nemani, S.; Yieh, E.; Kummel, A. C. Inherent Selective Pulsed Chemical Vapor Deposition of Aluminum Oxide in nm Scale. *Appl. Surf. Sci.* **2023**, *622*, 156824.

(28) Cho, Y.; Ahles, C. F.; Choi, J. Y.; Huang, J.; Jan, A.; Wong, K.; Nemani, S.; Yieh, E.; Kummel, A. C. Inherently Selective Water-Free Deposition of Titanium Dioxide on the Nanoscale: Implications for Nanoscale Patterning. *ACS Appl. Nano Mater.* **2022**, *5*, 476−485.

(29) (a) Cottrell, T. L. *The Strengths of Chemical Bonds*, 2nd ed., Butterworth: London, 1958 (b) Darwent, B. d. *National Standard Reference Data Series*; National Bureau of Standards, no. 31: Washington, 1970 (c) Benson, S. W. *J. Chem. Educ.* **1965**, *42*, 502. (d) Kerr, J. A. *Chem. Rev.* **1966**, *66*, 465.

(30) Yu, P.; Merkx, M. J. M.; Tezsevin, I.; Hausmann, D. M.; Sandoval, T.; Kessels, W. M. M.; Mackusa, A. J. M. Area-Selective ALD Using Small Molecule Inhibitors of Different Sizes: Steric Shielding Versus Chemical Passivation. *ASD2022*, 2022; p 28.

(31) Merkx, M. J. M.; Tezsevin, I.; Heinemans, R. H. G. M.; Lengers, R. J.; Kessels, W. M. M.; Sandoval, T. E.; Mackusa, A. J. M. Mechanisms of Precursor Blocking by Aniline Inhibitor Molecules During Area-Selective ALD of TaN. *ASD2022*, 2022; p 15.

(32) Andruniow, T.; Zgierski, M. Z.; Kozlowski, P. M. Theoretical Determination of the Co-C Bond Energy Dissociation in Cobalamins. *J. Am. Chem. Soc.* **2001**, *123*, 2679−2680.

(33) Moulder, C. A.; Cundari, T. R. A DFT Survey of the Effects of d-Electron Count and Metal Identity on the Activation and Functionalization of C−H Bonds for Mid to Late Transition Metals. *Isr. J. Chem.* **2017**, *57*, 1023−1031.

(34) Moulder, C. A.; Kafle, K.; Cundari, T. R. Tungsten-Ligand Bond Strengths for 2p Elements Including σ- And π-Bond Strength Components, A Density Functional Theory and ab Initio Study. *J. Phys. Chem. A* **2019**, *123*, 7940−7949.

(35) Huang, J.; Cho, Y.; Zhang, Z.; Jan, A.; Wong, K. T.; Nemani, S. D.; Yieh, E.; Kummel, A. C. Selective Pulsed Chemical Vapor Deposition of Water-Free TiO2/Al2O3 and HfO2/Al2O3 Nanolaminates on Si and SiO2 in Preference to SiCOH. *ACS Appl. Mater. Interfaces* **2022**, *14*, 15716−15727.